Reduction of the Pea Ferredoxin-NADP(H) Reductase Catalytic Efficiency by the Structuring of a Carboxyl-Terminal Artificial Metal Binding Site†

Daniela L. Catalano-Dupuy, Martín Orecchia, Daniela V. Rial, and Eduardo A. Ceccarelli*

Molecular Biology Division, Instituto de Biología Molecular y Celular de Rosario, Facultad de Ciencias Bioquímicas y Farmacéuticas, Universidad Nacional de Rosario, Suipacha 531, S2002LRK Rosario, Argentina

Received June 9, 2006; Revised Manuscript Received August 29, 2006

ABSTRACT: Ferredoxin (flavodoxin)-NADP(H) reductases (FNRs) are ubiquitous flavoenzymes that deliver NADPH or low-potential one-electron donors (ferredoxin, flavodoxin, and adrenodoxin) to redox-based metabolisms in plastids, mitochondria, and bacteria. The FNRs from plants and most eubacteria constitute a unique family, the plant-type ferredoxin-NADP(H) reductases. Plastidic FNRs are quite efficient at sustaining the demands of the photosynthetic process. At variance, FNRs from organisms with heterotrophic metabolisms or anoxygenic photosynthesis display turnover numbers that are 20−100-fold lower than those of their plastidic and cyanobacterial counterparts. To gain insight into the FNR structural features that modulate enzyme catalytic efficiency, we constructed a recombinant FNR in which the carboxyl-terminal amino acid (Tyr308) is followed by an artificial metal binding site of nine amino acids, including four histidine residues. This added structure binds Zn^{2+} or Co^{2+} and, as a consequence, significantly reduces the catalytic efficiency of the enzyme by decreasing its k_{cat}. The K_m for NADPH and the K_d for $NADP^+$ were increased 2 and 3 times, respectively, by the addition of the amino acid extension in the absence of Zn^{2+}. Nevertheless, the structuring of the metal binding site did not change the K_m for NADPH or the K_d for $NADP^+$ of the FNR-tail enzyme. Our results provide experimental evidence which indicates that mobility of the carboxyl-terminal backbone region of the FNR, mainly Tyr308, is essential for obtaining an FNR enzyme with high catalytic efficiency.

Ferredoxin (flavodoxin)-NADP(H) oxidoreductases (FNR1, EC 1.18.1.2) are an extensive distributed class of flavoenzymes that utilize the noncovalently bound FAD cofactor as the redox center. FNRs[1] participate in a wide variety of redox-based metabolisms by transferring electrons between obligatory one- and two-electron carriers, thus functioning as a general electronic splitter. In nonphototrophic bacteria and eukaryotes, the reaction is driven toward ferredoxin reduction, providing reducing power for multiple metabolic pathways, including steroid hydroxylation in mammalian mitochondria, nitrite reduction, and glutamate synthesis in heterotrophic tissues of vascular plants. These enzymes are also involved in radical propagation and scavenging in *Escherichia coli* and other prokaryotes and hydrogen and nitrogen fixation in anaerobes (for reviews, see refs *1* and *2*).

Several three-dimensional structures of FNRs have been determined (*3*−*11*). They show that these enzymes always contain two different domains, an antiparallel β-barrel that makes up the core for FAD binding in the amino-terminal region of the flavoprotein and a carboxyl-terminal domain that contains the $NADP^+$ binding site, with a characteristic α-helix−β-strand region that folds back into the FAD site. It has also been observed that other enzymes which are built using this FNR-like module contain additional amino or carboxyl domains which extend their enzymatic capabilities (*12*).

Several key issues have attracted attention to these enzymes in the past years. The terminal tyrosine (Tyr308 in pea FNR) has been shown to be responsible for substrate specificity (*13, 14*). This residue is conserved in all plant-type plastidic FNRs stacked coplanar to the *re* face of the isoalloxazine moiety making extensive interactions with it (refs *1*, *2*, and *12* and references therein). During enzyme turnover, the nicotinamide ring is required to go also onto the *re* face of the isoalloxazine moiety to permit the electron transfer between the cofactor and the substrate. Thus, Karplus and co-workers (*4*) have proposed that the aromatic side chain of the carboxyl-terminal tyrosine should be displaced to allow the substrate to move into the correct position. This process results in a decrease in the binding affinity for NADP(H) relative to those of the 2′-P-AMP and 2′-P-ADP-ribose analogues (*13*, *15*, *16*). The stacking of the terminal tyrosine onto the isoalloxazine weakens the interaction between the nicotinamide and the prosthetic group, increasing the relevance of the interactions which allows the enzyme to discriminate between NADP(H) and NAD(H).

† This study was supported by grants from CONICET and Agencia de Promoción Científica y Tecnológica (ANPCyT, Argentina). E.A.C. is a staff member of the Consejo Nacional de Investigaciones Científicas y Técnicas (CONICET, Argentina). D.L.C.-D. and D.V.R. are Fellows of CONICET.

* To whom correspondence should be addressed. E-mail: ceccarelli@ibr.gov.ar. Fax: 54-341-4390465. Phone: 54-341-4351235/4350596, ext. 145.

[1] Abbreviations: FNR, ferredoxin (flavodoxin)-NADP(H) reductase; Fd, ferredoxin; DCPIP, 2,6-dichlorophenolindophenol; GST, glutathione *S*-transferase; FNR-tail, recombinant pea FNR containing a carboxyl-terminal extension of nine amino acids that generates a metal binding site.

10.1021/bi061152v CCC: $33.50
Published on Web 10/31/2006

The involvement of the C-terminal residue has also been implicated in enzyme catalytic efficiency. Plant-type FNRs can be classified into a plastidic class that is characterized by an extended FAD conformation and high catalytic efficiency, and into a bacterial class that displays a folded FAD molecule and has low turnover rates (*1*, *17*). Turnover numbers in the range of 100−600 s^{-1} have been reported for *Anabaena*, *Chlamydomonas reinhardtii*, and chloroplast FNRs (*2*). On the other hand, bacterial reductases exhibit low efficiencies because of a severe decrease in the k_{cat} values, whereas the K_m values for NADP(H), Fd, and Fld remain in the low micromolar range for all reductases (*2*). In the chloroplastic and cyanobacterial reductases, as with most flavoproteins, the FAD molecule binds in an extended form, and the AMP moiety interacts with a short sheet−loop−sheet motif (*4*−*8*). At variance, in the bacterial FNRs, the adenosine of FAD bends backward such that the nitrogen at position 7 of the adenine group forms a hydrogen bond to nitrogen 1 of the isoalloxazine (*9*−*11*). This interaction is further stabilized by stacking of the adenosine onto an aromatic side chain of a tryptophan or a phenylalanine, which is positioned after the tyrosine that faces the isoalloxazine, homologous to Tyr308 from pea FNR. From this arrangement, one can suggest that movement of the amino acid facing the isoalloxazine is constrained and may be one of the determinants of the low catalytic efficiency of these bacterial enzymes.

The role of the terminal tyrosine in plant FNRs has been thoroughly studied. Its contribution to catalysis, in the modulation of the FAD reduction potential and in the inter- and intraprotein electron transfer processes, has been demonstrated (*13*, *14*, *16*, *18*, *19*). Participation of the above-mentioned tyrosine in these processes, as well as in the determination of specificity and the high catalytic efficiency, clearly suggests that this residue needs to have freedom and that its displacement may be essential for its functions, which has been proposed by several authors (*4*, *13*−*16*). However, no direct physical evidence of this motility has been obtained. Recently, using NMR, it has been shown that Tyr314 from maize FNR, in addition to the carboxyl-terminal region of the protein, is perturbed upon $NADP^+$ binding (*20*).

In an effort to provide evidence of the mentioned displacement, we constructed a mutant FNR in which Tyr308 is followed by an artificial metal binding site composed of nine amino acids, including four histidine residues. In the presence of a metal ion, this added structure folds itself and, as a consequence, may impair carboxyl-terminal backbone movement. This mutant FNR exhibited a decline in enzyme catalytic efficiency in the presence of either Zn^{2+} or Co^{2+}. The K_m for NADPH and the K_d for $NADP^+$ were increased 2 and 3 times, respectively, by the addition of the amino acid extension but were not affected by Zn^{2+} binding. Our results provide experimental evidence that freedom of the carboxyl-terminal backbone region of FNR, mainly Tyr308 motility, is essential for obtaining high enzyme catalytic efficiency.

MATERIALS AND METHODS

Protein Expression and Purification. Wild-type pea FNR was overexpressed in *E. coli* as reported previously (*21*) using vector pGF205+ (*22*). This vector expresses a GST−FNR fusion protein that contains a thrombin recognition site between the carboxyl terminus of GST and the first amino acid of mature FNR. Purification of the protein from *E. coli* JM109 was carried out as described previously (*21*). The mutant pea FNR containing a metal binding site (FNR-tail) was obtained by expression in *E. coli* using plasmid pGF105H. Briefly, the pGF105H expression vector containing the coding sequence for the mature pea ferredoxin-$NADP^+$ reductase followed by 30 bp of extra sequence was constructed as follows. The C-terminal half of the coding sequence for mature ferredoxin-$NADP^+$ reductase was amplified by PCR using the oligonucleotides FNR460 (5′-gacaagaatggcaagcctcacaa-3′) and FNRtail (5′-ttagaattcagtgagcgtgagcccaagcgtgagcgtgatagacttcaacgttccattgc-3′) as primers and vector pCV105 (*23*) as a template. To facilitate the cloning process, an *Eco*RI restriction site was introduced into the FNRtail primer. After amplification, the product (~683 bp) was digested with *Nhe*I and *Eco*RI enzymes and the resultant fragment was ligated into the pGF205+ vector (*22*) digested with the same enzymes, yielding plasmid pGF105H. Mutant pea FNR-tail was purified basically as follows. FNR-tail expression was performed without addition of EDTA to the culture medium. Then, the recombinant enzyme was purified from the cell extracts by affinity chromatography using Ni−NTA agarose (QIAGEN). Protein was eluted with 100 mM imidazole and digested with the endoprotease thrombin to separate FNR-tail from the GST carrier protein. FNR-tail was then chromatographed in a DEAE Macroprep column (2.5 cm × 50 cm, Bio-Rad) equilibrated in 50 mM HEPES (pH 8). The column was extensively washed with the same buffer, and bound FNR-tail was eluted using a 0 to 0.4 M linear gradient of NaCl in 50 mM HEPES (pH 8). Finally, purified samples were dialyzed against 50 mM HEPES (pH 8) previously treated with Chelex. Mutant FNR Tyr308Ser was purified as described previously (*15*, *19*).

Recombinant pea ferredoxin was obtained via expression in *E. coli* using vector pET28-Fd (*21*). This vector allows for the expression of pea ferredoxin in *E. coli* as a soluble protein with a high yield. Fd purification was performed essentially as described previously (*24*).

Protein Expression Assays. FNR-tail expression was analyzed under different growth conditions. In all cases, *E. coli* cells were growth in 10 mL of LB broth supplemented with 100 μg/mL ampicillin and 20 μM $ZnSO_4$ or EDTA at variable concentrations (0.1, 1.0, 5.0, and 10 mM). After induction of the culture with 1 mM IPTG at 30 °C for 2.5 h, cells were collected. The protein extracts were separated by SDS−PAGE and visualized with Coomassie Brilliant Blue R-250 stain or Western blotting (*25*, *26*), using anti-FNR antibodies that were produced in rabbits.

Colorimetric Zn^{2+} Concentration Binding Assay. To determine the amount of Zn^{2+} bound to FNR-tail and FNR, a colorimetric assay using 4-(2-pyridylazo)resorcinol (PAR) was performed (*27*). The recombinant protein was incubated with 80 μM $ZnSO_4$ for 20 min on ice. Then, the sample was filtered through a G25 Sephadex spin column. The amount of protein in the eluted sample was determined; it was then mixed with guanidine-HCl (final concentration of 8 M) and incubated at room temperature for 10 min. Then, samples were mixed with a freshly prepared PAR solution (final concentration of 100 μM), and absorbance spectra were recorded. The Zn^{2+} concentration was estimated by the

maximum emission intensity at 500 nm (corrected for the buffer) as compared with calibration experiments using zinc solutions of known concentrations (from 1 to 10 μM).

Spectral Analyses. Absorption spectra were recorded on a Shimadzu UV-2450 spectrophotometer. The nicotinamide ring occupancy of the binding site in FNR-tail was estimated from the absorbance spectrum change produced after addition of $NADP^+$. FNR-tail and FNR Tyr308Ser samples were diluted in 50 mM HEPES (pH 8) to a final concentration of ~15 μM. Absorption spectra were recorded at 25 °C both before and after the addition of 300 μM $NADP^+$, either in the absence or in the presence of 20 μM $ZnSO_4$. The mutant Tyr308Ser shows a very stable interaction between nicotinamide and the enzyme-binding site. Therefore, it has been assumed that substrate occupancy is 100% at a saturating $NADP^+$ concentration (*13*). Then, we compared the absorbance differences (ΔA at 515 nm) obtained with FNR Tyr308Ser and mutant FNR with the metal binding site, and we estimated the nicotinamide ring occupancy of the binding site in the latter.

The flavin fluorescence was monitored using a Varian Cary Eclipse fluorescence spectrophotometer interfaced with a personal computer. The solution for fluorescence measurements contained ~1 μM protein in 50 mM HEPES (pH 8). The samples were previously filtered through a desalting column. FAD fluorescence ($\lambda_{exc} = 445$ nm; $\lambda_{em} = 500-600$ nm) was registered both before and after the addition of 300 μM $NADP^+$ or 30 μM $ZnSO_4$ at 25 °C.

Activity Measurements. FNR-dependent diaphorase activity was determined by a published method (*28*). The reaction mixture (1 mL) contained 50 mM HEPES (pH 8), 3 mM glucose 6-phosphate, 0.3 mM $NADP^+$, 1 unit of glucose-6-phosphate dehydrogenase, and 0.033 mM dichlorophenolindophenol (DCPIP). After the addition of ~20 nM pea FNR, the reactions were monitored spectrophotometrically by following DCPIP reduction at 600 nm ($\epsilon_{600} = 21$ mM^{-1} cm^{-1}). The effect of metal on enzyme activity was analyzed by adding different concentrations of $ZnSO_4$ or $CoSO_4$ to the reaction medium.

The cytochrome *c* reductase activity of FNR was assayed in reaction medium (1 mL) containing 50 mM HEPES (pH 8), 0.3 mM NADPH, 50 μM cytochrome *c*, and 5 μM Fd. After the addition of ~15 nM FNR, the reaction was monitored spectrophotometrically to follow cytochrome *c* reduction at 550 nm ($\epsilon_{550} = 19$ mM^{-1} cm^{-1}). This activity was also assayed in the presence of 30 μM $ZnSO_4$.

All kinetic experiments were performed at 30 °C.

Determination of Kinetic Parameters. For the estimation of kinetic parameters of the diaphorase reaction, measurements were carried out at different $NADP^+$ concentrations, at a fixed saturating concentration of DCPIP, in both the absence and presence of 30 μM $ZnSO_4$ in the case of mutant FNR. Steady-state kinetic data were fitted to the theoretical curves using SIGMAPLOT (Systat Software Inc., Point Richmond, CA).

Determination of the Dissociation Constant of the FNR·$NADP^+$ Complex. To determine the K_d value of the complex between FNR and $NADP^+$, ~15 μM flavoprotein in 50 mM HEPES (pH 8) was titrated at 25 °C with the substrate. After each addition, the absorbance spectrum (300−600 nm) was monitored using a Shimadzu UV-2450 spectrophotometer. Then, difference spectra were calculated and the absorbance differences (ΔA at 515 nm) were plotted against $NADP^+$ concentrations. Data were fitted to a theoretical equation for a 1:1 complex using the nonlinear regression program included in SIGMAPLOT to optimize the K_d value. The effect of Zn^{2+} on the K_d value of this complex for mutant FNR was also determined. The experimental setup was as described above, except that 20 μM $ZnSO_4$ was included in the solution.

Determination of the Dissociation Constants of the FNR-Tail·Zn^{2+} Complex. To determine K_d values for binding of Zn^{2+} to FNR-tail, the sample was excited at 295 nm, and the fluorescence emission was scanned from 300 to 450 nm. Spectra were obtained for solutions containing each enzyme at 2 μM with increasing concentrations of $ZnSO_4$ of up to 60 μM in 50 mM HEPES (pH 8) at 25 °C. Emission data at 344 nm were fitted to the theoretical equation for a 1:1 stoichiometric complex by means of nonlinear regression.

Molecular Graphics. The computer graphics are based on X-ray diffraction data for the pea enzyme (*15*) using Swiss-PdbViewer 3.7 (SP5) and rendered with POV-Ray. The model of the metal binding site was generated using the conjugate gradient method of Fletcher−Reeves to achieve final convergence available in Hyperchem 6.01.

RESULTS

Design and Construction of an Artificial Metal Binding Site at the Carboxyl Terminus of FNR. Ferredoxin-$NADP^+$ reductase was converted into a Zn^{2+} binding protein via the addition of a nine-amino acid extension to its carboxyl terminus. We decided to construct a site composed of only histidines to avoid the experimental difficulties resulting from the inclusion of cysteines. The first histidine was introduced immediately after Tyr308 to maximize the perturbation that the added amino acid extension may introduce upon metal binding. Alanines were placed around histidines to favor some plasticity of the peptide in the absence of metals. When the amino acid extension was analyzed using intrinsic protein disorder prediction software (*29*), residues were assigned as belonging to loops, which can be taken as an indication of disorder (not shown). In the central region of the designed peptide, a tryptophan surrounded by two alanines was included to force the peptide to fold back which facilitates metal binding. Furthermore, the aromatic amino acid allows an internal signal to be tracked for the assessment of binding of metal to the artificial site (Figure 1A).

A predicted structure was obtained using Hyperchem and a Fletcher−Reeves geometry optimization assuming that the four histidines were involved in metal binding and using only the allowed torsional angles (Figure 1B). We are aware of the possible existence of different binding structures. Not all possible sequence and rotamer combinations were explored because this analysis was out of the scope of this work. A cartoon representation of the structures of pea FNR with the added peptide in an open extended form without metal bound and a hypothetical folded form with Zn^{2+} are shown in Figure 1C. The cartoon suggests the probable change upon binding of metal to the amino acid tail with respect to the entire protein. Figure 1D shows a hypothetical composed drawing of the NADP(H)·FNR complex in which only FAD, the added extra amino acids in an extended form, and $NADP^+$ were included. This simulation was performed

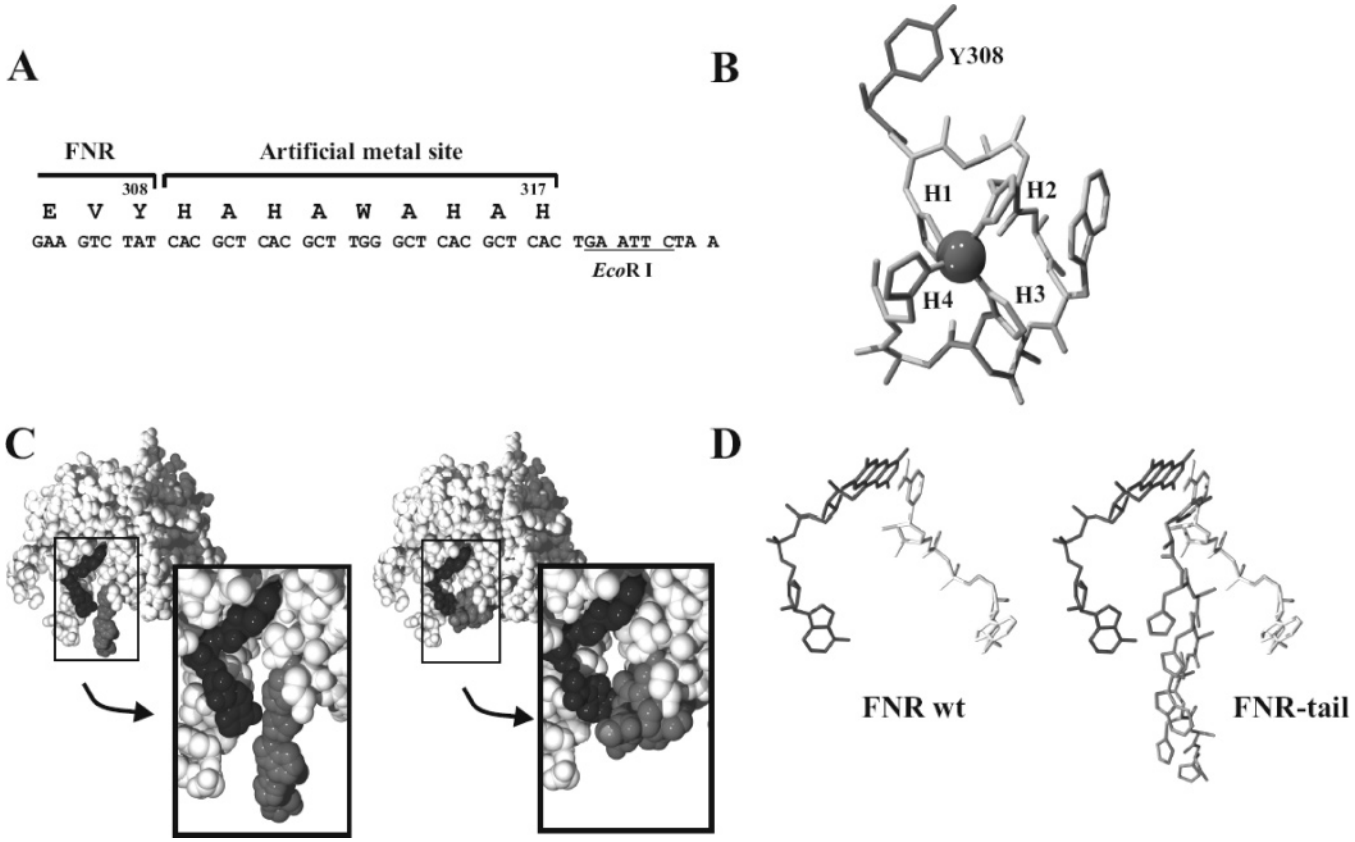

FIGURE 1: Design of the artificial metal binding site. (A) Sequence of the carboxyl-terminal region of FNR-tail, including the last three FNR residues and the nine additional amino acids. (B) Predicted structure of the artificial metal binding site obtained using Hyperchem and a Fletcher−Reeves geometry optimization assuming that the four histidines (H1, H2, H3, and H4) were involved in metal binding. The gray sphere represents the zinc ion. (C) Cartoon representation structure of pea FNR with the added peptide in an open extended form (left) and a hypothetical folded form with bound Zn^{2+} (right). The FAD and the metal binding site are colored black and dark gray, respectively. (D) Hypothetical composed drawing of the $NADP^+$·FNR-tail complex. This simulation was performed by fitting the crystallographic structure of the wild-type and mutant Tyr308Ser·$NADP^+$ FNRs and the metal binding site, considering the orientation of Tyr308. Only FAD (dark gray), $NADP^+$ (light gray), and the artificial metal binding site in an extended form (gray) are shown.

by fitting the crystallographic structure of the wild type and the Tyr308Ser FNR mutant with $NADP^+$ bound plus the metal binding tail, considering the orientation of Tyr308. This allows us to envisage that the added amino acid tail does not directly affect the binding site for NADP(H).

Expression, Purification, and Characterization of FNR-Tail. The presence of FNR polypeptides in induced *E. coli* cells expressing the recombinant protein was studied by SDS−PAGE (Figure 2). Inclusion of 20 μM $ZnSO_4$ in the culture medium resulted in a marked impairment of recombinant enzyme solubility (Figure 2A, lanes 4−6). From these cells, marginally low levels of the active enzyme were recovered by glutathione agarose chromatography when compared to the purification performed from *E. coli* cells expressing the protein in a culture medium lacking the addition of Zn^{2+} and in the presence of EDTA (compare lanes 3 and 6 of Figure 2A). On the other hand, inclusion of Zn^{2+} during expression of the wild-type enzyme did not alter its solubility (not shown). The addition of EDTA to the culture medium during induction of protein expression increased the fraction of soluble recombinant protein, but it reduced the protein expression levels (Figure 2B). The protein produced as a GST amino-terminal fusion was partially recovered in the supernatant as a ca. 60 kDa product similar to those of the wild-type flavoprotein fused to the same carrier protein. Digestion with thrombin produced a recombinant FNR-tail 1 kDa greater in size than the wild-type enzyme, which is expected with the addition of a nine-amino acid extension (Figure 2C).

We observed that FNR-tail strongly interacted with Ni−agarose resin and eluted as a single peak with 100 mM imidazole. Under identical conditions, wild-type FNR did not bind to the metal affinity column. Thus, metal affinity chromatography was introduced as the first purification step of the GST−FNR-tail fusion protein as described in Materials and Methods. Purified FNR-tail was active, contained no bound metals, and was >99% pure as observed by SDS−PAGE and Coomassie Brilliant Blue staining (Figure 2D). FNR-tail displayed the characteristic flavoprotein absorption spectra (see below) and was stable while frozen at −70 °C for months. When the protein was electrophoresed on standard nondenaturing polyacrylamide gels and stained for the determination of enzymatic activity, both wild-type FNR and recombinant FNR-tail were detected as single active bands. Inclusion of 20 μM Zn^{2+} in the sample and all electrophoresis buffers did not produce any protein aggregation and resulted in an only small change in enzyme mobility and a lower activity (data not shown).

Metal Binding. Total binding of Zinc was assessed for the wild-type enzyme and for FNR-tail using 4-(2-pyridylazo)-resorcinol (PAR) as described in Materials and Methods. As shown in Table 1, FNR-tail was able to retain $\sim 0.55 \pm 0.05$ mol of Zn^{2+} per mole of polypeptide after filtration through a G25 Sephadex spin column, whereas no Zn^{2+} was found

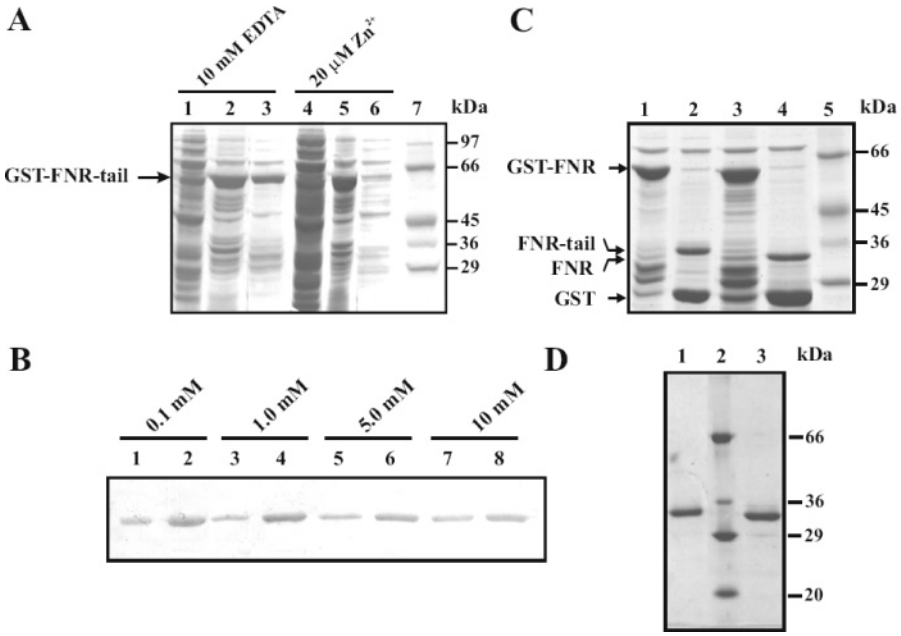

FIGURE 2: Expression and purification of FNR-tail. (A) FNR-tail expression in induced *E. coli* cells was studied by SDS−PAGE. Cells were grown in LB medium supplemented with 100 μg/mL ampicillin, and either 10 mM EDTA or 20 μM $ZnSO_4$. The soluble fraction was in lanes 1 and 4; the insoluble fraction was in lanes 2 and 5, and enzyme recovered by glutathione−agarose chromatography was in lanes 3 and 6. (B) Effect of the addition of different EDTA concentrations (0.1, 1.0, 5.0, and 10.0 mM) to the culture medium during induction of protein expression on FNR-tail solubility. SDS−PAGE was followed by Western blotting using anti-pea FNR antibody. Soluble fractions were in lanes 1, 3, 5, and 7; insoluble fractions were in lanes 2, 4, 6, and 8. (C) Wild-type FNR and FNR-tail were obtained as GST amino-terminal fusions: lane 1, GST−FNR-tail; lane 3, GST−FNR. Then, they were digested with thrombin: lane 2, FNR-tail; lane 4, wild-type FNR. (D) Purified FNRs: lane 1, FNR-tail; lane 2, molecular weight markers; lane 3, wild-type FNR.

Table 1: Effects of Metal Binding on the Kinetic Parameters of the Wild-Type and Recombinant Forms of Pea FNR

FNR form	mol of Zn^{2+}/mol of polypeptide[a]	K_d[b] (μM, Zn^{2+})	K_d[c] (μM, $NADP^+$)	nicotinamide ring occupancy of the binding site (%)[c]	cytochrome *c* reductase activity[d] (μmol mg^{-1} min^{-1})	K_m[d] (μM, NADPH)	k_{cat}[d] (s^{-1})	k_{cat}/K_m[d] (μM^{-1} s^{-1})
wild-type FNR	−	ND[e]	32 ± 2.3	14	30.5 ± 1.5	1.2 ± 0.1	74.1 ± 5.9	61.7
FNR-tail	−	ND[e]	97 ± 19	10	29.2 ± 1.7	2.4 ± 0.2	73.5 ± 5.1	30.6
FNR-tail with Zn^{2+}	0.55 ± 0.05	2.1 ± 0.4	100 ± 22	10	5.3 ± 0.3	2.6 ± 0.2	10.1 ± 0.7	3.8

[a] Metal bound to the protein after filtration and centrifugation through Sephadex G25. [b] Data obtained from Figure 3. [c] Data obtained as described in Materials and Methods. [d] Each value represents the average of three independent experiments. [e] Not determined.

to be associated with the wild-type enzyme. Then, we tested if the fluorescence properties of the tryptophan included in the metal binding site displayed environmental sensitivities related to metal binding. Pea FNR contains six tryptophans, none of which are directly involved in the prosthetic group or NADP(H) binding. Tryptophans 52 and 176 are partially exposed to the environment. All others are buried inside the protein structure. When fluorescence emission spectra were recorded with an excitation of 295 nm, only subtle changes were detected for the wild-type protein upon addition of 60 μM Zn^{2+} (Figure 3A). FNR-tail displayed an increase in fluorescence with a maximum at 344 nm (Figure 3B). Using these experimental conditions and different concentrations of the metal, we calculated a dissociation constant of 2.1 ± 0.4 μM for binding of Zn^{2+} to the FNR-tail protein, assuming 1 mol of metal per mole of polypeptide. The obtained K_d value was similar to that obtained with a GST fusion protein containing only the artificial metal binding site fused to its carboxyl terminus through a 19-amino acid peptide linker (not shown). This observation supports the contention that the site folds upon Zn^{2+} binding. The artificial metal binding site displays a high affinity for Zn^{2+}, suggesting the original design was appropriate for the proposed analysis.

Spectral Properties of FNR-tail and Interaction with $NADP^+$ and NAD^+. We first performed spectral analysis of the purified FNR-tail enzyme, which had been treated with Chelex or 1 mM EDTA to avoid interference of any trace metals. The protein displayed a typical FNR spectrum with maxima at 385 and 459 nm and shoulders at 430 and 470 nm (Figure 4A). The 275 nm:459 nm spectral ratio was between 8 and 8.9, indicating that the purified recombinant enzyme contains one FAD per molecule of apoprotein. A FAD:polypeptide stoichiometry of 0.95 was also calculated by FAD release in the presence of 0.2% SDS (*30*). Therefore, the addition of the small carboxyl-terminal metal binding domain neither prevents assembly of the prosthetic group nor impedes the production of a folded protein, although, as we mentioned above, the folded metal binding site may affect the protein folding process. Then, we carried out the same analysis by adding 40 μM $ZnSO_4$. As shown in Figure 4B, only subtle changes were detected.

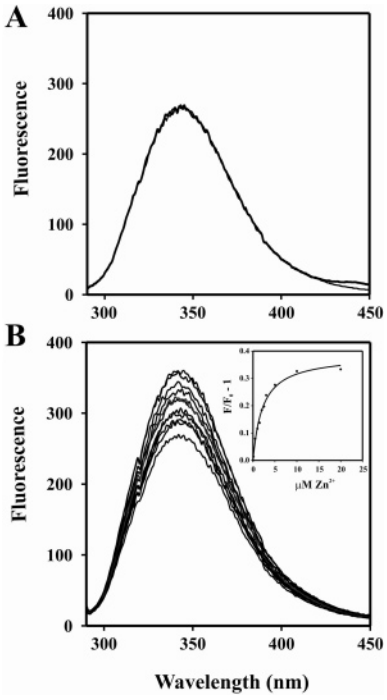

FIGURE 3: Determination of K_d values for binding of Zn^{2+} to FNR-tail. (A) Fluorescence emission spectra (λ_{exc} = 295 nm) registered with 2 μM wild-type FNR both before and after addition of 60 μM Zn^{2+}. (B) Fluorescence spectra (λ_{exc} = 295 nm) obtained during titration of 2 μM FNR-tail with Zn^{2+} (0−60 μM $ZnSO_4$). The inset shows emission data at 344 nm that were fitted to the theoretical equation for a 1:1 stoichiometric complex by means of nonlinear regression. The determined K_d value was 2.1 μM.

We investigated the capacity of FNR-tail to interact with pyridine nucleotides either in the absence or in the presence of Zn^{2+}, under conditions in which the metal binding site is completely folded. As shown in panels B and C of Figure 4, $NADP^+$ elicited the same spectral change when bound to the FNR-tail enzyme in both the absence and presence of Zn^{2+}, indicating that metal binding site folding did not alter the interaction of $NADP^+$ with the prosthetic group. Titration experiments with $NADP^+$ and NAD^+ were performed to determine the affinity of recombinant FNR for ligands and the effect of Zn^{2+} addition. The K_d values obtained for the FNR-tail·$NADP^+$ complex, either in the absence or in the presence of 40 μM Zn^{2+}, were both the same and higher than that obtained for the wild-type enzyme (Table 1). In the case of NAD^+, the K_d values for the complex with either wild-type FNR, FNR-tail, or Zn^{2+}-bound FNR-tail were too high to be appropriately measured with the methods employed, and no spectral differences were detected with a NAD^+ final concentration of up to 2 mM. However, in both cases, a K_d of >2 mM is expected. Thus, it can be concluded that the structuring of the metal binding site did not increase the affinity of the enzyme for NAD^+.

Piubelli et al. (*13*) defined a degree of nicotinamide occupancy of $NADP^+$ bound to FNR, assuming that the complex of FNR Tyr308Ser with $NADP^+$ has 100% occupancy. Then, the occupancies of any FNR·$NADP^+$ complex can be estimated by comparison of the spectral changes at 515 nm between the enzyme under study and the mutant FNR Tyr308Ser. When we analyzed recombinant FNR-tail, we obtained values that indicate a similar occupancy for the recombinant enzyme in the absence and presence of Zn^{2+}

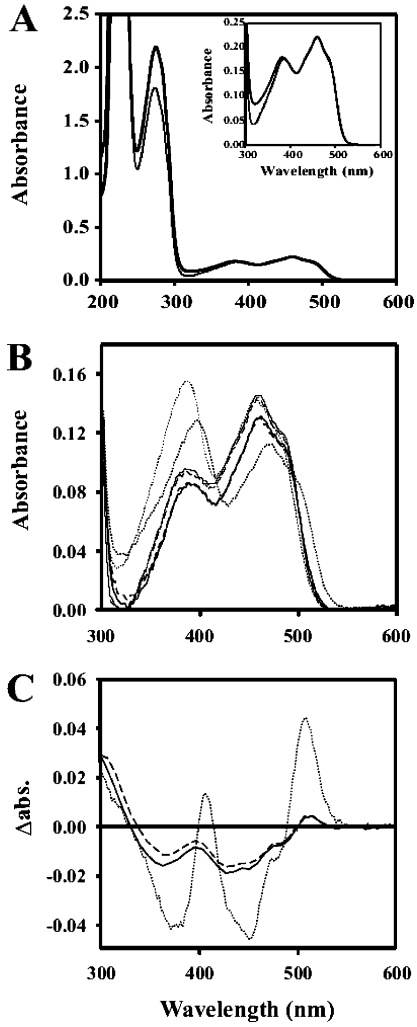

FIGURE 4: Spectral properties of FNR. (A) Absorbance spectra of wild-type FNR (thin line) and FNR-tail (thick line). The inset shows an amplified view of the region between 300 and 600 nm. (B) Absorption spectra of FNR-tail, obtained in either the absence (dashed lines) or presence (solid lines) of 40 μM Zn^{2+}, and mutant FNR Tyr308Ser (dotted lines) monitored both before (thin lines) and after (thick lines) the addition of 300 μM $NADP^+$. (C) Differential spectra elicited by the binding of $NADP^+$ obtained from the absorption spectra depicted in panel B.

(10%, Table 1). These values are similar to those obtained for wild-type FNR [14% (this work and refs *13* and *16*)].

The environment of bound FAD in FNR-tail was probed by measuring the intrinsic flavin fluorescence of the protein. The fluorescence emission spectra are shown in Figure 5. The fluorescence of bound FAD is known to be largely quenched in the native oxidized form of wild-type FNR (*31*). We observed that the emission of both FNR and FNR-tail flavoenzymes at 524 nm were ~0.5−0.7% of that of free FAD if measured immediately after gel filtration (not shown). FNR-tail displayed only small increases in the relative quantum yields in the absence of Zn^{2+}. Addition of 30 μM Zn^{2+} caused an increase in fluorescence (Figure 5A), indicating that the structuring of the metal binding site altered the interaction between Tyr308 and the isoalloxazine ring. It has been reported that FNR undergoes FAD fluorescence enhancement upon formation of a complex with $NADP^+$ (*18*, *31*, *32*). Following addition of the nucleotide, an increase in quantum yield was observed for FNR-tail. The amplitude of the increase in fluorescence obtained by $NADP^+$ addition

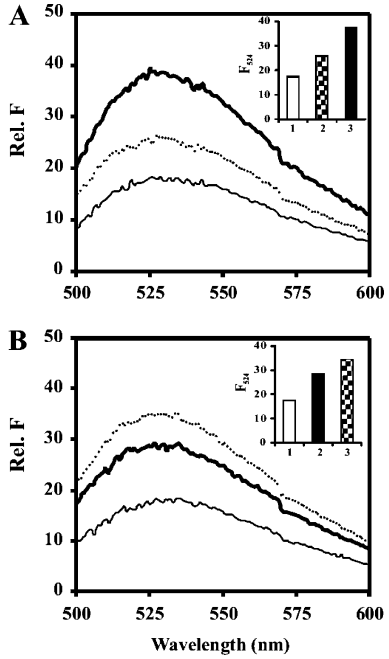

FIGURE 5: FAD fluorescence of FNR. Fluorescence emission spectra of FNR-tail (λ_{exc} = 445; λ_{em} = 500−600 nm) monitored both before (thin line) and after successive additions of (A) 30 μM Zn^{2+} (dotted line) and 300 μM $NADP^+$ (thick line) or (B) 300 μM $NADP^+$ (thick line) and 30 μM Zn^{2+} (dotted line). Insets shows fluorescence emission data at 524 nm: (A) lane 1, FNR-tail; lane 2, FNR-tail and 30 μM Zn^{2+}; lane 3, FNR-tail and 30 μM Zn^{2+} and then 300 μM $NADP^+$; and (B) lane 1, FNR-tail; lane 2, FNR-tail and 300 μM $NADP^+$; lane 3, FNR-tail and 300 μM $NADP^+$ and then 30 μM Zn^{2+}.

was equivalent for the FNR-tail in both the absence and presence of Zn^{2+}. The fluorescence enhancements observed with the addition of $NADP^+$ and Zn^{2+} to FNR-tail were approximately additive relative to those observed with each one, separately. These results suggest that, in both cases, the fluorescence enhancements were caused by breakdown of the stacked interaction between the flavin and aromatic side chain at position 308, and the processes are probably independent of each other (Figure 5A,B).

Enzyme Activities and Steady-State Kinetics of FNR-Tail. The effect of metals on recombinant FNR enzymatic activity is shown in Figure 6. DCPIP diaphorase activity was decreased via the addition of increasing concentrations of $ZnSO_4$. DCPIP diaphorase activity was chosen because we have previously determined that $ZnSO_4$ inhibits FNR in the presence of ferrocyanide, the product of the ferricyanide diaphorase activity of the enzyme (*21*). Addition of Co^{2+} also affected the activity of the recombinant enzyme, but to a lesser extent. None of the metals affected the activity of the wild-type enzyme under the same conditions. NADPH oxidation, catalyzed by the FNR-tail enzyme using ferredoxin (Fd) as an electron acceptor, was also affected by the presence of Zn^{2+}, but no inhibition was observed using the wild-type enzyme (Table 1). Thus, it may be inferred that binding of metal to the histidine rich extension affects enzyme activity.

To further investigate the relative changes in the enzyme upon metal binding, the catalytic activity using NADPH and DCPIP as a function of pH was analyzed. In the absence of any metal, FNR-tail displayed a pH profile similar to that obtained for the wild-type enzyme. In parallel, we analyzed

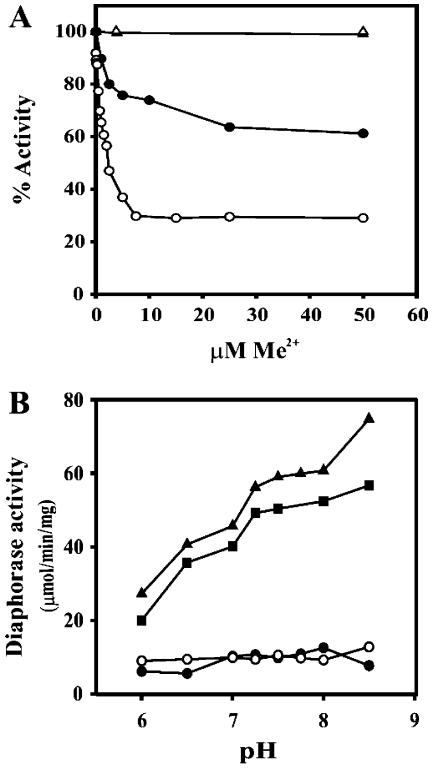

FIGURE 6: Effect of the presence of metal on the diaphorase activity of the FNR-tail enzyme. (A) NADPH-DCPIP diaphorase activity was assayed in both the absence and presence of increasing $ZnSO_4$ (○) or $CoSO_4$ (●) concentrations (from 0 to 50 μM) in the reaction medium. The effect of the metal on wild-type FNR diaphorase activity was also assayed under the same conditions (△ and ▲). (B) NADPH-DCPIP diaphorase activity was assayed as a function of pH using wild-type FNR (▲), mutant FNR Tyr308Ser (○) and FNR-tail both with (●) and without (■) 20 μM Zn^{2+}.

the activity profile of pea FNR Tyr308Ser. Both the mutant enzyme that lacks an aromatic amino acid stacked on the isoalloxazine and FNR-tail containing bound Zn^{2+} exhibited a shallow increase in activity as a function of pH (Figure 6B).

The steady-state kinetics showed that FNR-tail in the absence of metal displayed an identical k_{cat} value for the diaphorase activity using NADPH and DCPIP; meanwhile, an increase of 100% in the K_m for the nucleotide was observed (from 1.2 to 2.4 μM) with respect to that of the wild-type enzyme (Table 1). When the kinetic parameters were obtained in the presence of Zn^{2+}, a substantial decrease in k_{cat} was observed and no changes were detected for K_m with respect to that of the recombinant enzyme in the absence of the metal.

Thus, the structuring of the metal binding site produces neither an alteration of $NADP^+$ binding nor detectable changes in nicotinamide occupancy. Moreover, the K_m of the recombinant enzyme remains unchanged, whereas a significant decrease in k_{cat} was observed upon metal binding; as shown in Table 1, a 16-fold decrease in catalytic efficiency was observed under the conditions that were tested.

DISCUSSION

The significant role of the C-terminal Tyr in the enzyme function of plant-type ferredoxin-$NADP^+$ reductases has been firmly documented (*13*, *14*, *16*). Aromatic amino acids have also been identified as being stacked over the isoalloxazine

in other FNRs and closely related flavoenzymes (*10*, *11*, *33*, *34*). This role has also been suggested for nitric oxide synthase (*35*, *36*) and cytochrome P450 reductase (*37*−*39*). The obtained crystal structures of mutant and wild-type enzymes containing bound $NADP^+$ suggest that the phenol side chain of the terminal tyrosine has to be moved out to allow nicotinamide to be situated in a position compatible with the electron transfer process (*6*, *14*, *15*). However, Tyr movement had never been documented, and unfortunately, it has not been possible to obtain crystal data showing the orientations of the above-mentioned Tyr and the nicotinamide during productive substrate binding. The obtained data indicate that the terminal Tyr of FNR may have more than one role during substrate binding and catalysis (*13*, *14*, *16*, *18*, *19*). This issue is still not settled and needs to be addressed further. The carboxyl-terminal Tyr strongly influences the enzyme specificity for NADPH by destabilizing the interaction of nicotinamide, the common moiety of both nucleotides NAD^+ and $NADP^+$ (*13*, *14*, *16*). A similar observation was recently made for flavocytochrome P450 BM3 from *Bacillus megaterium* (*39*). Similarly, the FAD shielding residue, Phe1395, of the neuronal nitric oxide synthase, an enzyme which contains a FAD/NADPH subdomain that belongs to the FNR family (*12*), facilitates $NADP^+$ release (*36*). This aromatic amino acid prevents release of the nucleotide from being rate-limiting and enables the substrate to modulate a conformational equilibrium that controls the electron transfer of another subdomain which contains FMN. In the same way, the terminal Tyr of FNR decreases the affinity of the enzyme for the nucleotide, allowing for fast dissociation of the substrate after hydride transfer that would otherwise remain bound, thus preventing another steady-state enzyme cycle (*14*, *16*). Removal and substitution of the Tyr by site-directed mutagenesis have proven that this amino acid is by no means essential for catalysis (*2*), but it is important for enzyme catalytic efficiency optimization. The precise mechanism in which Tyr308 participates in these functions is still not completely understood. Some bacterial reductases, like *E. coli* FNR, have a Tyr residue equivalent to Tyr308 that faces the isoalloxazine. However, turnover numbers of these enzymes are at least 1000 times lower than those observed for the plastidic FNRs, while their K_m and K_d values for substrates remain in the same range (ref *2* and references therein). In these bacterial reductases, the Tyr is followed by a short amino acid stretch that interacts with the adenine moiety of FAD, which is bound in a twisted conformation. This arrangement probably reduces the carboxyl-terminal movement of the protein.

In this work, we have examined whether it is possible to modify the catalytic efficiency of FNR by restricting the motility of the carboxyl-terminal region. By constructing an artificial metal binding site next to Tyr308 of pea FNR, we were able to examine some of the different roles of Tyr308. We present here the first experimental evidence that the backbone conformational freedom at the C-terminus of FNR is related to the enzyme catalytic efficiency.

Histidine-based metal binding sites have been identified in nature and have been introduced into artificial metal binding peptides (*40*−*50*). In those proteins, the metal ion controls the backbone conformation and the arrangement of the R groups of the involved amino acids, which produces defined structures. By adding a nine-amino acid extension, containing the sequence HAHAWAHAH, we converted pea FNR into a metal binding enzyme. Since the added peptide extension is structured by metal binding, perturbations should occur in the immediately preceding Tyr308, thus restricting its ability to spontaneously and independently move. In the absence of metal, the added tail should be flexible and, as predicted in silico, does not contain a rigid secondary structure.

Changes in tryptophan fluorescence in response to conformational perturbation allowed us to monitor that the artificial metal binding site introduced in FNR binds Zn^{2+} at micromolar concentrations. Neither changes in tryptophan fluorescence nor metal binding was detected in the wild-type enzyme. Moreover, the analysis of the pea FNR crystal structure showed that no histidine or cysteines are close enough to participate in metal binding with the added extension. Four acidic residues, Glu272, Asp276, Asp277, and Asp171, are in the proximity, but only the last two may be accessible for metal binding in conjunction with the added histidines. Thus, it can be suggested that the effects observed by the addition of metal to FNR-tail are related to the structuring of the amino acid extension, although it is not possible to preclude possible interactions with other surface residues of the protein. The structuring effect is valid in any case. We measured ~0.55 mol of bound Zn^{2+} per mole of enzyme. The stoichiometry was lower than expected, which may be due to the method employed which involves Sephadex filtration. Filtration and centrifugation through the matrix may reverse the equilibrium by decreasing the amount of metal bound to the protein if the metal−protein complex rapidly reaches equilibrium. However, the obtained value indicates that at least 1 mol of Zn^{2+} binds to the protein under the conditions that were tested. The K_d of 2.1 μM for the FNR-tail·Zn^{2+} complex obtained by analyzing the protein fluorescence emission spectra is in agreement with the formation of a rigid metal binding site with the involvement of more than one histidine. This structuring should affect carboxyl-terminal motility. Correspondingly, it has been suggested that an alternatively spliced N-terminal variable region of troponin T with a HxxxH core sequence modulates the conformation and flexibility of another protein domain through metal binding (*50*).

Previous results have shown that nonconservative mutations at the C-terminal position of pea and *Anabaena* FNRs produce extremely high affinities for $NADP^+$ and generate the ability of the enzyme to bind NAD^+ and catalyze reactions with it (*13*, *14*, *16*, *18*). The changes observed in those mutants probably occur because Tyr308 modulates the thermodynamics of nicotinamide binding. When we analyzed the K_d for binding of $NADP^+$ to FNR-tail, we observed that the structuring of the metal binding site did not influence the affinity of the recombinant enzyme for the nucleotide. Thus, it can be inferred that Tyr308 is still controlling $NADP^+$ binding under both conditions. Moreover, binding of metal to FNR-tail enhanced the intrinsic flavin fluorescence, but it remained lower than that produced by $NADP^+$. The fluorescence enhancement produced by nucleotide binding is thought to originate from displacement of Tyr308 from the isoalloxazine (*18*). In that context, it has been determined that only ~14% of the population of FNR with bound $NADP^+$ had the nicotinamide stacked over the

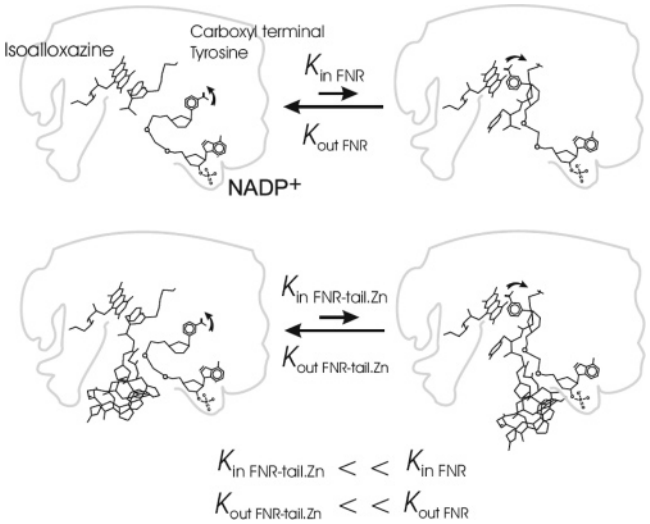

FIGURE 7: Schematic representation of the bipartite NADP(H) binding mode. The model is based on previously proposed models (*14*). The steps of NADP(H) binding through the adenine, pyrophosphate, and 2′-phosphate bound to the enzymes were omitted for simplicity. The model proposes that decreasing the motility of the carboxyl-terminal region by metal binding affects both constants to a similar extent. See the text for details.

isoalloxazine, which produces the fluorescence enhancement observed upon nucleotide binding, whereas the enhancement directed by metal binding comes from all FNR-tail molecules. Thus, we can conclude that if some rearrangement of the terminal tyrosine and the isoalloxazine occurs upon structuring of the metal binding site, this change should be relatively minor with respect to that produced by the nucleotide. Moreover, the structuring of the artificial tail did not affect the fluorescence enhancement that was induced by the substrate. Thus, Tyr308 undergoes a rearrangement upon binding of $NADP^+$ to the FNR-tail enzyme in the presence of Zn^{2+} similar to that in the wild-type enzyme. One plausible explanation for our observations is that the equilibrium between nicotinamide and the terminal tyrosine is equivalent but is reached more slowly upon structuring of the metal binding site. Therefore, the K_{in} and K_{out} values for binding of nicotinamide to the binding site would be equally affected (see Figure 7).

Using NMR techniques, it has been determined that the carboxyl-terminal polypeptide chain of FNR is particularly flexible and conformational changes of these regions probably favor opening of the active sites (*20*). Recently, a detailed study on binding of NADPH to cytochrome P450 reductase has been performed (*51*). The FAD binding domain of this enzyme belongs to the FNR family, while the FMN binding domain is related to flavodoxins (*52*). The determination of energetic contributions indicates that binding of coenzyme to the FAD subdomain can drive a global conformational change of the enzyme that affects the FMN domain (*51*). Thus, binding of $NADP^+$ to FNR may be able to drive a conformational change that includes the carboxyl-terminal region. The calculated catalytic constants (Table 1) indicate that the catalytic efficiency decrease is directly related to metal binding. These results suggest that the motility of the carboxyl-terminal region, which has been put under structural constraints, affects enzyme catalysis. Meanwhile, the K_d and K_m of the enzyme are the same for the FNR-tail enzyme in either the absence or the presence of Zn^{2+}, and the structuring of the metal binding site severely decreased the catalytic efficiency of the FNR-tail enzyme, which is mainly due to a reduction in k_{cat}. A mechanism in which the tyrosine flips "in" and "out" of the pocket has been anticipated (*4*, *13*−*15*). Recently, Tejero et al. (*14*) proposed that this movement would create an equilibrium between the in and out conformations of tyrosine, where the in conformation is the one in which the nicotinamide is in the proper position and, then, it is the reactive species (see Figure 7). A slow equilibrium between both conformations would convert the reactive species in a bottleneck. If the equilibrium mentioned above exists, it should proceed in a short time scale to be not rate-limiting. The equilibrium constants obtained by these authors clearly support the proposed hypothesis. Our data also support this model. The structuring of the carboxyl-terminal region by metal binding probably decreases both K_{in} and K_{out} similarly and produces a considerable alteration of the catalytic efficiency, as we detected. We think that these results are the first evidence of physical movement of the tyrosine. Moreover, the data presented here support the idea that local backbone motion of the carboxyl-terminal region is necessary to obtain the observed efficiency in plant-type FNRs. Thus, two different functions of the carboxyl-terminal regions may be envisaged. One is directly related to the adjustment of nucleotide affinity by the inclusion of an aromatic ring facing the isoalloxazine, thus blocking the ability of the nicotinamide to strongly interact with it. The other function is to ensure the rapid exchange of the nicotinamide in and out of the active site through local backbone movement. The freedom that evolution has developed in plastidic reductases for its carboxyl-terminal backbone is restricted in bacterial-type FNRs. The typical folded FAD, which allows for stacking of its adenine with an aromatic side chain (Trp248 in the case of *E. coli*), probably results in the low mobility of the carboxyl-terminal region and thus results in enzymes with low catalytic efficiencies.

The concerted studies of this recombinant FNR, other mutants, and wild-type enzymes, as well as the generation of new crystal data, will allow these issues to be better understood.

REFERENCES

1. Ceccarelli, E. A., Arakaki, A. K., Cortez, N., and Carrillo, N. (2004) Functional plasticity and catalytic efficiency in plant and bacterial ferredoxin-NADP(H) reductases, *Biochim. Biophys. Acta 1698*, 155−165.
2. Carrillo, N., and Ceccarelli, E. A. (2003) Open questions in ferredoxin-$NADP^+$ reductase catalytic mechanism, *Eur. J. Biochem. 270*, 1900−1915.
3. Karplus, P. A., Daniels, M. J., and Herriott, J. R. (1991) Atomic structure of ferredoxin-$NADP^+$ reductase: Prototype for a structurally novel flavoenzyme family, *Science 251*, 60−66.
4. Bruns, C. M., and Karplus, P. A. (1995) Refined crystal structure of spinach ferredoxin reductase at 1.7 Å resolution: Oxidized, reduced and 2′-phospho-5′-AMP bound states, *J. Mol. Biol. 247*, 125−145.
5. Serre, L., Vellieux, F. M., Medina, M., Gomez-Moreno, C., Fontecilla-Camps, J. C., and Frey, M. (1996) X-ray structure of the ferredoxin:$NADP^+$ reductase from the cyanobacterium *Anabaena* PCC 7119 at 1.8 Å resolution, and crystallographic studies of $NADP^+$ binding at 2.25 Å resolution, *J. Mol. Biol. 263*, 20−39.
6. Hermoso, J. A., Mayoral, T., Faro, M., Gomez-Moreno, C., Sanz-Aparicio, J., and Medina, M. (2002) Mechanism of coenzyme recognition and binding revealed by crystal structure analysis of

ferredoxin-NADP$^+$ reductase complexed with NADP$^+$, *J. Mol. Biol. 319*, 1133−1142.
7. Dorowski, A., Hofmann, A., Steegborn, C., Boicu, M., and Huber, R. (2000) Crystal structure of paprika ferredoxin-NADP$^+$ reductase: Implications for the electron transfer pathway, *J. Biol. Chem. 276*, 9253−9263.
8. Kurisu, G., Kusunoki, M., Katoh, E., Yamazaki, T., Teshima, K., Onda, Y., Kimata-Ariga, Y., and Hase, T. (2001) Structure of the electron transfer complex between ferredoxin and ferredoxin-NADP$^+$ reductase, *Nat. Struct. Biol. 8*, 117−121.
9. Nogues, I., Perez-Dorado, I., Frago, S., Bittel, C., Mayhew, S. G., Gomez-Moreno, C., Hermoso, J. A., Medina, M., Cortez, N., and Carrillo, N. (2005) The Ferredoxin-NADP(H) Reductase from *Rhodobacter capsulatus*: Molecular Structure and Catalytic Mechanism, *Biochemistry 44*, 11730−11740.
10. Ingelman, M., Ramaswamy, S., Niviere, V., Fontecave, M., and Eklund, H. (1999) Crystal structure of NAD(P)H:flavin oxidoreductase from *Escherichia coli*, *Biochemistry 38*, 7040−7049.
11. Sridhar, P. G., Kresge, N., Muhlberg, A. B., Shaw, A., Jung, Y. S., Burgess, B. K., and Stout, C. D. (1998) The crystal structure of NADPH:ferredoxin reductase from *Azotobacter vinelandii*, *Protein Sci. 7*, 2541−2549.
12. Karplus, P. A., and Bruns, C. M. (1994) Structure-function relations for ferredoxin reductase, *J. Bioenerg. Biomembr. 26*, 89−99.
13. Piubelli, L., Aliverti, A., Arakaki, A. K., Carrillo, N., Ceccarelli, E. A., Karplus, P. A., and Zanetti, G. (2000) Competition between C-terminal tyrosine and nicotinamide modulates pyridine nucleotide affinity and specificity in plant ferredoxin-NADP$^+$ reductase, *J. Biol. Chem. 275*, 10472−10476.
14. Tejero, J., Perez-Dorado, I., Maya, C., Martinez-Julvez, M., Sanz-Aparicio, J., Gomez-Moreno, C., Hermoso, J. A., and Medina, M. (2005) C-Terminal Tyrosine of Ferredoxin-NADP$^+$ Reductase in Hydride Transfer Processes with NAD(P)$^+$/H, *Biochemistry 44*, 13477−13490.
15. Deng, Z., Aliverti, A., Zanetti, G., Arakaki, A. K., Ottado, J., Orellano, E. G., Calcaterra, N. B., Ceccarelli, E. A., Carrillo, N., and Karplus, P. A. (1999) A productive NADP$^+$ binding mode of ferredoxin-NADP$^+$ reductase revealed by protein engineering and crystallographic studies, *Nat. Struct. Biol. 6*, 847−853.
16. Nogues, I., Tejero, J., Hurley, J. K., Paladini, D., Frago, S., Tollin, G., Mayhew, S. G., Gomez-Moreno, C., Ceccarelli, E. A., Carrillo, N., and Medina, M. (2004) Role of the C-terminal tyrosine of ferredoxin-nicotinamide adenine dinucleotide phosphate reductase in the electron transfer processes with its protein partners ferredoxin and flavodoxin, *Biochemistry 43*, 6127−6137.
17. Arakaki, A. K., Ceccarelli, E. A., and Carrillo, N. (1997) Plant-type ferredoxin-NADP$^+$ reductases: A basal structural framework and a multiplicity of functions, *FASEB J. 11*, 133−140.
18. Calcaterra, N. B., Pico, G. A., Orellano, E. G., Ottado, J., Carrillo, N., and Ceccarelli, E. A. (1995) Contribution of the FAD binding site residue tyrosine 308 to the stability of pea ferredoxin-NADP$^+$ oxidoreductase, *Biochemistry 34*, 12842−12848.
19. Orellano, E. G., Calcaterra, N. B., Carrillo, N., and Ceccarelli, E. A. (1993) Probing the role of the carboxyl-terminal region of ferredoxin-NADP$^+$ reductase by site-directed mutagenesis and deletion analysis, *J. Biol. Chem. 268*, 19267−19273.
20. Maeda, M., Lee, Y. H., Ikegami, T., Tamura, K., Hoshino, M., Yamazaki, T., Nakayama, M., Hase, T., and Goto, Y. (2005) Identification of the N- and C-terminal substrate binding segments of ferredoxin-NADP$^+$ reductase by NMR, *Biochemistry 44*, 10644−10653.
21. Catalano Dupuy, D. L., Rial, D. V., and Ceccarelli, E. A. (2004) Inhibition of pea ferredoxin-NADP(H) reductase by Zn-ferrocyanide, *Eur. J. Biochem. 271*, 4582−4593.
22. Rial, D. V., Arakaki, A. K., and Ceccarelli, E. A. (2000) Interaction of the targeting sequence of chloroplast precursors with Hsp70 molecular chaperones, *Eur. J. Biochem. 267*, 6239−6248.
23. Ceccarelli, E. A., Viale, A. M., Krapp, A. R., and Carrillo, N. (1991) Expression, assembly, and processing of an active plant ferredoxin-NADP$^+$ oxidoreductase and its precursor protein in *Escherichia coli*, *J. Biol. Chem. 266*, 14283−14287.
24. Hurley, J. K., Salamon, Z., Meyer, T. E., Fitch, J. C., Cusanovich, M. A., Markley, J. L., Cheng, H., Xia, B., Chae, Y. K., and Medina, M. (1993) Amino acid residues in *Anabaena* ferredoxin crucial to interaction with ferredoxin-NADP$^+$ reductase: Site-directed mutagenesis and laser flash photolysis, *Biochemistry 32*, 9346−9354.
25. Maniatis, T., Fritsch, E. F., and Sambrook, J. (1982) *Molecular cloning. A laboratory manual*, Cold Spring Harbor Laboratory Press, Plainview, NY.
26. Towbin, H., Staehelin, T., and Gordon, J. (1979) Electrophoretic transfer of proteins from polyacrylamide gels to nitrocellulose sheets: Procedure and some applications, *Proc. Natl. Acad. Sci. U.S.A. 76*, 4350−4354.
27. McCall, K. A., Huang, C., and Fierke, C. A. (2000) Function and mechanism of zinc metalloenzymes, *J. Nutr. 130*, 1437S−1446S.
28. Zanetti, G. (1976) A lysyl residue at the NADP$^+$ binding site of ferredoxin-NADP$^+$ reductase, *Biochim. Biophys. Acta 445*, 14−24.
29. Linding, R., Jensen, L. J., Diella, F., Bork, P., Gibson, T. J., and Russell, R. B. (2003) Protein disorder prediction: Implications for structural proteomics, *Structure 11*, 1453−1459.
30. Aliverti, A., Bruns, C. M., Pandini, V. E., Karplus, P. A., Vanoni, M. A., Curti, B., and Zanetti, G. (1995) Involvement of serine 96 in the catalytic mechanism of ferredoxin-NADP$^+$ reductase: Structure−function relationship as studied by site-directed mutagenesis and X-ray crystallography, *Biochemistry 34*, 8371−8379.
31. Shin, M. (1973) Complex formation by ferredoxin-NADP$^+$ reductase with ferredoxin or NADP$^+$, *Biochim. Biophys. Acta 292*, 13−19.
32. Zanetti, G., and Forti, G. (1966) Studies on the triphosphopyridine nucleotide-cytochrome *f* reductase of chloroplasts, *J. Biol. Chem. 241*, 279−285.
33. Correll, C. C., Ludwig, M. L., Bruns, C. M., and Karplus, P. A. (1993) Structural prototypes for an extended family of flavoprotein reductases: Comparison of phthalate dioxygenase reductase with ferredoxin reductase and ferredoxin, *Protein Sci. 2*, 2112−2133.
34. Wang, M., Roberts, D. L., Paschke, R., Shea, T. M., Masters, B. S., and Kim, J. J. (1997) Three-dimensional structure of NADPH-cytochrome P450 reductase: Prototype for FMN- and FAD-containing enzymes, *Proc. Natl. Acad. Sci. U.S.A. 94*, 8411−8416.
35. Adak, S., Sharma, M., Meade, A. L., and Stuehr, D. J. (2002) A conserved flavin-shielding residue regulates NO synthase electron transfer and nicotinamide coenzyme specificity, *Proc. Natl. Acad. Sci. U.S.A. 99*, 13516−13521.
36. Konas, D. W., Zhu, K., Sharma, M., Aulak, K. S., Brudvig, G. W., and Stuehr, D. J. (2004) The FAD-shielding residue Phe1395 regulates neuronal nitric-oxide synthase catalysis by controlling NADP$^+$ affinity and a conformational equilibrium within the flavoprotein domain, *J. Biol. Chem. 279*, 35412−35425.
37. Gutierrez, A., Paine, M., Wolf, C. R., Scrutton, N. S., and Roberts, G. C. (2002) Relaxation kinetics of cytochrome P450 reductase: Internal electron transfer is limited by conformational change and regulated by coenzyme binding, *Biochemistry 41*, 4626−4637.
38. Gutierrez, A., Doehr, O., Paine, M., Wolf, C. R., Scrutton, N. S., and Roberts, G. C. (2000) Trp-676 facilitates nicotinamide coenzyme exchange in the reductive half-reaction of human cytochrome P450 reductase: Properties of the soluble W676H and W676A mutant reductases, *Biochemistry 39*, 15990−15999.
39. Neeli, R., Roitel, O., Scrutton, N. S., and Munro, A. W. (2005) Switching pyridine nucleotide specificity in P450 BM3: Mechanistic analysis of the W1046H and W1046A enzymes, *J. Biol. Chem. 280*, 17634−17644.
40. Morgan, W. T. (1985) The histidine-rich glycoprotein of serum has a domain rich in histidine, proline, and glycine that binds heme and metals, *Biochemistry 24*, 1496−1501.
41. Brewer, D., and Lajoie, G. (2000) Evaluation of the metal binding properties of the histidine-rich antimicrobial peptides histatin 3 and 5 by electrospray ionization mass spectrometry, *Rapid Commun. Mass Spectrom. 14*, 1736−1745.
42. Waite, J. H., and Rice-Ficht, A. C. (1989) A histidine-rich protein from the vitellaria of the liver fluke *Fasciola hepatica*, *Biochemistry 28*, 6104−6110.
43. Waite, J. H., Vaccaro, E., Sun, C., and Lucas, J. M. (2002) Elastomeric gradients: A hedge against stress concentration in marine holdfasts? *Philos. Trans. R. Soc. London, Ser. B 357*, 143−153.
44. Hara, M., Fujinaga, M., and Kuboi, T. (2005) Metal binding by citrus dehydrin with histidine-rich domains, *J. Exp. Bot. 56*, 2695−2703.
45. Pelmenschikov, V., and Siegbahn, P. E. (2002) Catalytic mechanism of matrix metalloproteinases: Two-layered ONIOM study, *Inorg. Chem. 41*, 5659−5666.

46. Ladner, J. E., Obmolova, G., Teplyakov, A., Howard, A. J., Khil, P. P., Camerini-Otero, R. D., and Gilliland, G. L. (2003) Crystal structure of *Escherichia coli* protein ybgI, a toroidal structure with a dinuclear metal site, *BMC Struct. Biol. 3*, 7.
47. Moroz, O. V., Antson, A. A., Grist, S. J., Maitland, N. J., Dodson, G. G., Wilson, K. S., Lukanidin, E., and Bronstein, I. B. (2003) Structure of the human S100A12-copper complex: Implications for host-parasite defence, *Acta Crystallogr. D59*, 859−867.
48. Djalali, R., Chen, Y.-f., and Matsui, H. (2002) Au Nanowire Fabrication From Sequenced Histidine-Rich Peptide, *J. Am. Chem. Soc. 124*, 13660−13661.
49. Dwyer, M. A., Looger, L. L., and Hellinga, H. W. (2003) Computational design of a Zn^{2+} receptor that controls bacterial gene expression, *Proc. Natl. Acad. Sci. U.S.A. 100*, 11255−11260.
50. Jin, J. P., and Root, D. D. (2000) Modulation of troponin T molecular conformation and flexibility by metal ion binding to the NH_2-terminal variable region, *Biochemistry 39*, 11702−11713.
51. Grunau, A., Paine, M. J., Ladbury, J. E., and Gutierrez, A. (2006) Global effects of the energetics of coenzyme binding: NADPH controls the protein interaction properties of human cytochrome P450 reductase, *Biochemistry 45*, 1421−1434.
52. Porter, T. D., and Kasper, C. B. (1986) NADPH-cytochrome P-450 oxidoreductase: Flavin mononucleotide and flavin adenine dinucleotide domains evolved from different flavoproteins, *Biochemistry 25*, 1682−1687.

BI061152V